Locking Electric Differential for Brushless DC Machine-based Electric Vehicle with Independent Wheel Drives

M. Gougani, *Student Member, IEEE,* M. Chapariha, *Student Member, IEEE*, and J. Jatskevich, *Senior Member, IEEE*
The University of British Columbia, Department of Electrical and Computer Engineering
E-mails: {gougani, mehrdadc, jurij}@ece.ubc.ca

***Abstract* – The stability of vehicles under certain driving conditions is improved by forcing the wheels to turn at the same speed regardless of the available traction under individual wheels. For conventional vehicles this can be achieved by locking the mechanical differential system. This paper proposes an innovative approach for locking the electrical differential system (EDS) of electric vehicles (EV) with independent brushless DC (BLDC) machine-based wheel drives. The proposed method locks the active wheels of the vehicle as if they were operating on a common shaft. The locking algorithm is implemented by processing the Hall sensor signals of the considered motors and driving them with a single set of "averaged" Hall signals, thereby operating the motors at the same speed and angle. A detailed switch-level model of the EDS embedded with the proposed sync-lock control (SLC) along with the BLDC propulsion motors has been developed and compared against the measurements for the considered BLDC propulsion motors. The proposed technique is shown to achieve better results compared to a conventional speed control loop as the considered motors are locked directly through the corresponding magnetic fields.**

***Index Terms* – Average filtering, brushless dc motors, electric differential system, electric vehicle**

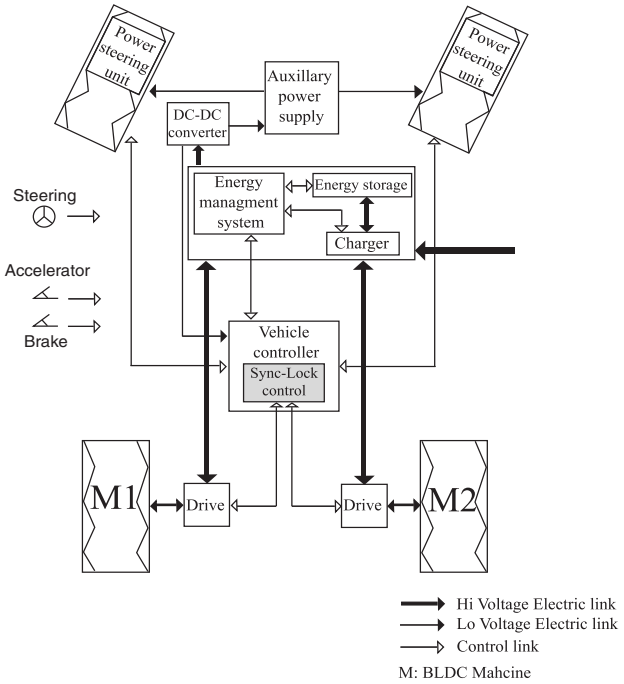

Fig. 1. Considered electric vehicle configuration.

I. INTRODUCTION

Locking the wheels' differential is commonly used in special purpose vehicles for achieving improved stability under uneven terrain and difficult driving conditions. The electric drive train considered in the paper is conceptually illustrated in Fig. 1. The drive train consists of three main subsystems: electric propulsion, energy source, and auxiliary systems [1]. The electric propulsion subsystem, which is the focus of this paper, is comprised of a vehicle controller, power electronic converters, and electric motors (driving wheels). The control inputs from the accelerator and brake pedal along with the steering are fed to the vehicle controller. The controller in turn operates the power electronic drive which regulates the power flow between the electric motor and the energy source. The energy source subsystem includes energy storage, energy management unit, and a charger. Finally, the auxiliary subsystem manages the power steering units and the interior auxiliary devices. Since in electrical vehicles similar to that depicted in Fig. 1 there is no common mechanical shaft or transmission that can be used for locking the wheels, this operation is achieved by the proposed Sync-Lock Control (SLC) that enables locking of the electrical differential system (EDS).

The considered vehicle propulsion system is based on typical brushless dc (BLDC) motors that are voltage-source-inverter (VSI) driven and controlled by the conventional Hall sensors. The details of the electric propulsion system of the vehicle are shown in Fig. 2. Without loss of generality two BLDC propulsion motors are assumed here, whereas the proposed SLC concept is readily extended for any number of driving wheels. To achieve the desired locking of the wheels, the conventional approach may be implemented using the proportional-plus-integral (PI) control loops to equalize the speed of both (or all) motors/wheels. In this paper, an innovative and alternative approach is proposed that is based on filtering the original Hall-sensor signals to produce a modified set of signals that is used to synchronize-lock both motors/inverters as depicted in Fig.2. The paper presents the EV propulsion system and shows that the proposed SLC of the EDS achieves better performance and improved locking over the conventional method.

978-1-61284-247-9/11/$26.00 ©2011 IEEE

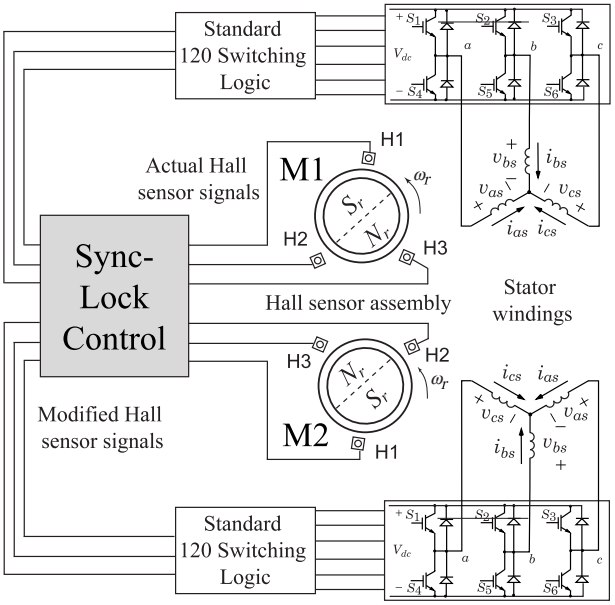

Fig. 2. BLDC motor-drive system.

II. Electric Vehicle Detailed Model

A. BLDC Propulsion System Model

BLDC machines are often considered in various electromechanical applications, and in general have been investigated quite well in the literature [2]–[5]. A detailed model of a BLDC machine shown in Fig. 3 is considered to be incorporated into the electric vehicle model. Based on the commonly used assumptions, the stator voltage equation may be expressed as [2]–[5]:

$$\mathbf{v}_{abcs} = \mathbf{r}_s \mathbf{i}_{abcs} + \frac{d\boldsymbol{\lambda}_{abcs}}{dt} \tag{1}$$

where $\mathbf{f}_{abcs} = [f_{as} \quad f_{bs} \quad f_{cs}]^T$ may represent the voltage, current or flux linkage vectors. Also, $\mathbf{r}_s$ represents the stator resistance matrix. In the case of a motor with non-sinusoidal back emf, the back emf is assumed to be half-wave symmetric and contains spatial harmonics. Therefore, the stator flux linkages and electromagnetic torque may be written as [5]:

$$\boldsymbol{\lambda}_{abcs} = L_s \mathbf{i}_{abcs} + \lambda'_m \sum_{n=1}^{\infty} K_{2n-1} \begin{bmatrix} \sin((2n-1)\theta_r) \\ \sin\left((2n-1)\left(\theta_r - \frac{2\pi}{3}\right)\right) \\ \sin\left((2n-1)\left(\theta_r + \frac{2\pi}{3}\right)\right) \end{bmatrix}, \tag{2}$$

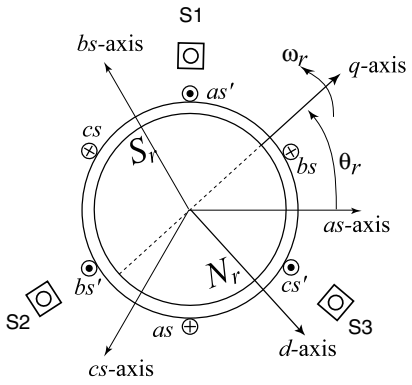

Fig. 3. Three phase BLDC machine with Hall sensors.

$$T_e = \frac{3P}{4} \lambda'_m \sum_{n=1}^{\infty} K_{2n-1} \begin{bmatrix} i_{as} \\ i_{bs} \\ i_{cs} \end{bmatrix}^T \cdot \begin{bmatrix} \cos((2n-1)\theta_r) \\ \cos\left((2n-1)\left(\theta_r - \frac{2\pi}{3}\right)\right) \\ \cos\left((2n-1)\left(\theta_r + \frac{2\pi}{3}\right)\right) \end{bmatrix}, \tag{3}$$

where L_s is the equivalent stator inductance, and λ'_m is the magnitude of the fundamental component of the permanent magnet (PM) magnet flux linkage. The coefficients K_n represent the magnitude of the n^{th} harmonic of the flux relative to fundamental component normalized such that $K_1 = 1$.

For the EV described in this paper, the prototype BLDC motors whose parameters are summarized in Appendix A are considered. The detailed model of the system was developed and implemented in MATLAB Simulink [6] using the toolbox [7]. The 120-degree inverter logic was implemented according to the standard table [4], [8], [9]. The model is verified by carrying out experiments using several commercially available BLDC Hall-sensor-based drivers as

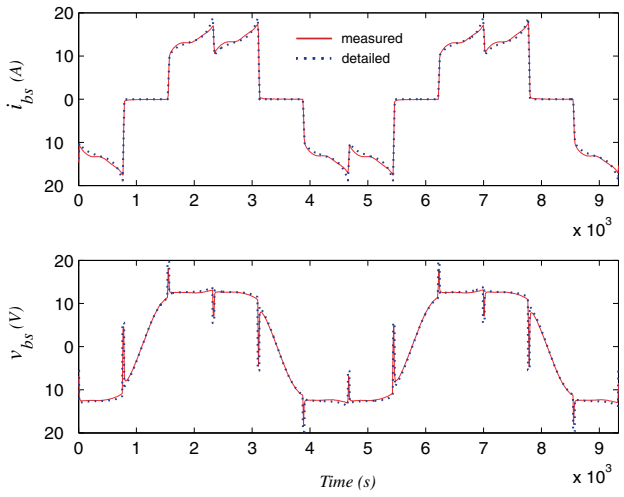

Fig. 4. Measured and simulated phase currents and voltages.

well as a prototype driver [10], all producing the same results. For this study, an operating point defined by a 330W mechanical load is considered. The motor inverter was supplied with $V_{dc} = 26V$, resulting in a speed of 2140 rpm under the given mechanical load. The measured phase currents and voltages were captured and are shown in Fig. 4. The simulated phase currents and voltages for the same steady state operating condition are also shown in Fig. 4. As can be seen, the detailed model predicts the phase currents and voltages very closely and agrees with the measured waveforms. This study confirms the accuracy of the developed detailed model, which is used in further studies.

A. Mechanical Subsystem and Vehicle Model

The mechanical subsystem consists of the vehicle body and the wheels system. The dynamics of the vehicle body motion, under the assumption of running on a flat profile, is assumed to have the following form

$$M\frac{dv}{dt} = F_m - R(v), \tag{4}$$

where M is the total vehicle and wheel mass, F_m is the drive force, g is the gravitational constant, v is the vehicle velocity and the running resistance, $R(v)$, is defined as [11]

$$R(v) = \left(1.867 + 0.0359v + 0.000745v^2\right)Mg/1000. \tag{5}$$

The dynamics of each drive-wheel-system may be expressed as

$$T_e = J\frac{d\omega_{rm}}{dt} + B_m\omega_{rm} + T_m, \tag{6}$$

where ω_{rm} is the rotor mechanical speed, J is the combined inertia of the wheel and the rotor, and B_m is the damping coefficient associated with the mechanical rotational system of the machine. Given r as the wheel radius, the mechanical load torque on each motor is

$$T_m = F_m r, \tag{7}$$

with the drive force defined by

$$\begin{aligned} F_m &= \mu(v_{slip})N \\ &= \mu(v_{slip})Mg, \end{aligned} \tag{8}$$

where μ is the adhesion coefficient described by the nonlinear function of slip velocity as follows [12]

$$\mu(v_{slip}) = a.\exp^{-b.v_{slip}} - c.\exp^{-d.v_{slip}}. \tag{9}$$

Here, the slip velocity defined as the difference between wheel and vehicle speed may be expressed as follows

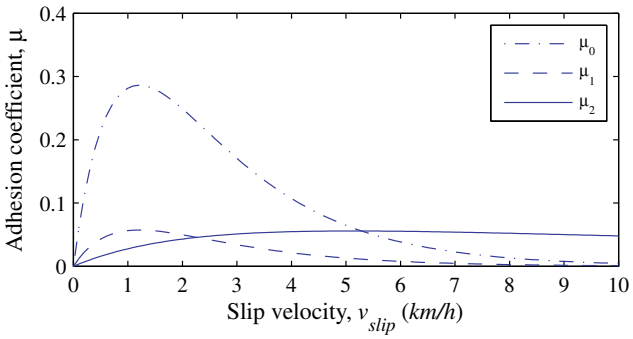

Fig. 5. Example of Adhesion coefficient-functions for dry and wet conditions.

TABLE I
SAMPLE ADHESION COEFFICIENT PARAMETERS

	a	*b*	*c*	*d*
μ_0 (dry)	1	0.54	1	1.2
μ_1 (wet 1)	0.2	0.54	0.2	1.2
μ_2 (wet 2)	0.08	0.05	0.08	0.5

$$v_{slip} = v_{wh} - v = r\omega_{rm} - v. \tag{10}$$

The adhesion coefficients corresponding to the parameters in Table 1 are illustrated in Fig. 5 as a function of slip velocity. The parameters a, b, c, and d are defined based on road surface conditions. Table 1 summarizes the parameters for three different conditions.

Having established both electrical and mechanical model of the propulsion system, different methodologies for locking the EDS can be objectively evaluated. It should be noted that the focus of the paper is on synchronization and locking of velocities of the motors rather than the aforementioned slip velocity.

III. SYNCHRONIZATION TECHNIQUES

A. Conventional Speed Control

Conventionally speed of a BLDC motor is controlled via an external speed control loop. The Hall sensors supply information about the position of the rotor and speed. If the speed of the motor drops because of an increase in load torque, the speed error increases, which in turn increases the voltage either by pulse width modulation (PWM). The two motors therefore can be coupled with identical reference speeds on the control systems as shown in Fig. 6 [13]. The mechanical block (i.e. vehicle body) is the link between the two motors. This conventional approach results in soft locking of the EDS, which does not enforce the same position of the rotors/wheels. In this method, the load experienced by one motor is only slightly felt by the other motor due to the change in the speed of the entire vehicle and the running resistance.

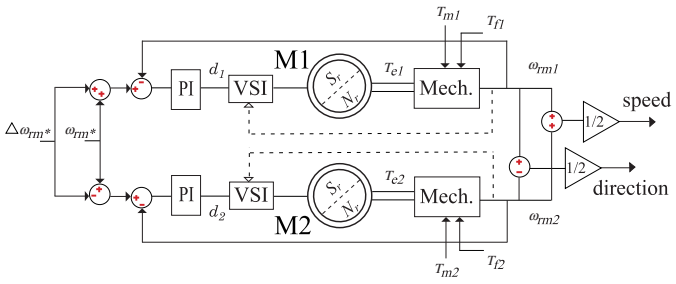

Fig. 6. Conventional EDS speed/torque control diagram.

B. *Proposed Sync-Lock Control*

The proposed Sync-Lock control strategy synchronizes the BLDC motors via the corresponding Hall sensor signals as depicted in Fig. 7. The filtering technique is based on the idea of driving both the motors with a set of "averaged" signals thereby locking speed and angle of both motors. The proposed locking strategy is different from a soft lock approach based on a PI controller as the two motors are locked internally by coupling the respective magnetic fields through Hall sensor signals.

To better understand how to filter the Hall-sensor signals, it is instructive to consider the diagram depicted in Fig. 8. When the motor is running, the Hall sensors produce square wave signals displaced by exactly 120 electrical degrees relative to each other. Combining all three outputs produces a square wave (see Fig. 8, top first and second signals) with a period equal to one-third of a Hall-sensor period, which is equal to 60 electrical degrees. The angular intervals between two successive switching events are denoted by $\theta(n)$. The durations of intervals $\theta(n)$ are denoted here by $\tau(n)$. Here, the angle φ denotes a possible delay or advance between rotors of the two motors [2].

The SLC is based on constructing one set of Hall signals by appropriately modifying (filtering) the signals from actual sensors $H_1\{1,2,3\}$ and $H_2\{1,2,3\}$. The proposed method works by first finding the rising edge correction interval $\tau_r^{corr}(n)$ by means of averaging the switching times $t(n)$ as follows:

$$\tau_r^{corr}(n) = \frac{1}{2}\left(t_r^{lag}(n) - t_r^{lead}(n)\right). \tag{11}$$

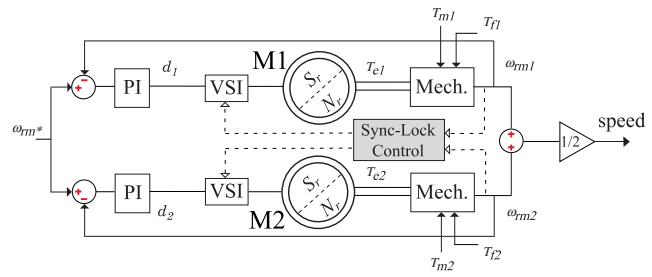

Fig. 7. EDS speed/torque control diagram with proposed SLC.

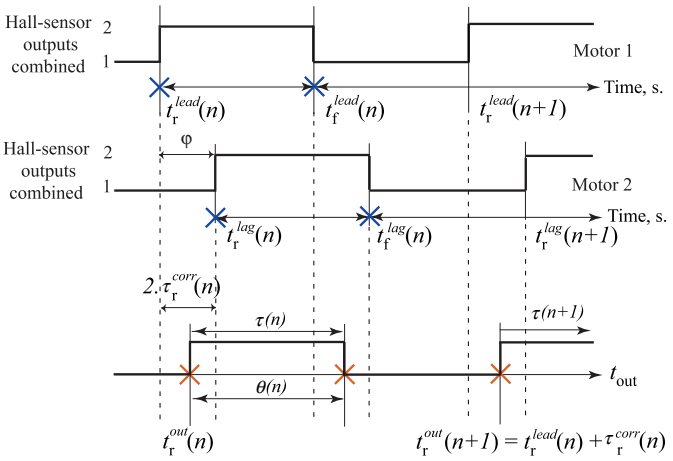

Fig. 8. Proposed averaging of the Hall sensor signals for SLC.

Once the correction value $\tau_r^{corr}(n)$ is established using the filter, the actual timing for commutating the inverter transistors for the next cycle can be found as follows:

$$t_r^{out}(n+1) = t_r^{lead}(n+1) + \tau_r^{corr}(n), \tag{12}$$

where $t_r^{lead}(n)$, the leading motors switching time, is defined as the reference switching time of the system. And the period of the average signal is calculated to be

$$\tau(n+1) = \tfrac{1}{2}\left(\left(t_f^{lead}(n) - t_r^{lead}(n)\right) + \left(t_f^{lag}(n) - t_r^{lag}(n)\right)\right). \tag{13}$$

IV. CASE STUDIES

In order to evaluate the performance of the proposed SLC, it was implemented using the detailed model of the EV described in Section II. In general, the proposed SLC can be implemented using either a programmable integrated circuit microcontroller, or using a combination of logic gates, integrators, and a flip flop. A detailed model of the proposed synchronization techniques has been developed and implemented in the BLDC motor-drive system.

In the following studies, the propulsion system supplied with $V_{dc} = 48V$. The coefficient, μ_0, of road surface friction defined by (9) is calculated with the parameters summarized in Table 1. The motion equations (4) and (6) are then determined by obtaining the drive force, F_m defined by (8). The PI controllers of the system have been fine-tuned to achieve satisfactory acceleration at the start up. The same controller coefficients are used for both differential systems. The coefficients along with the vehicle mechanical parameters are summarized in Appendix A.

B. *Sync-Lock Controller Transient*

To illustrate the enabling of the locking mechanism, the two motors are initially displaced by about 10 degrees and commanded to speed up to 100 rad/s (about 955 rpm). After

the start up transient the motors settle down at 25 degrees apart. When the SLC is enabled, the system undergoes transient as depicted in Fig. 9. This transient is due to the initial angle difference of the motor shafts, which causes one of the motors to accelerate and another motor to decelerate to achieve the locking. After that, both motors continue to operate at the same speed and angle synchronized as shown in Fig. 9. The common speed shown on the plot (Fig. 9, top subplot) is the referred mechanical (in rpm) of the virtual shaft driving the car forward. The slight difference in speed of the vehicle and the wheels is due to traction slip discussed in Section II B.

C. *Load-Step Transient*

Here, the performance of the locking mechanism is evaluated by subjecting the motors to a load disturbance. Fig. 10 shows the response of the conventional EDS, and Fig. 11 illustrates the speeds and electromagnetic torques of the two motors when the SLC is activated. Comparing Figs. 10 and 11, we can see that the difference in the speeds of the two motors is significantly improved with the proposed approach.

To see the improvement more clearly, Fig. 12 shows the angle difference between the motors' shafts. As it can be seen in this Figs. 11 and 12, the conventional synchronization of the EDS, although achieves the same speed, leads to significant difference between the shafts, which in a sense implies a "soft" synchronization. At the same time, the proposed SLC keeps the motor shafts aligned relative to each other.

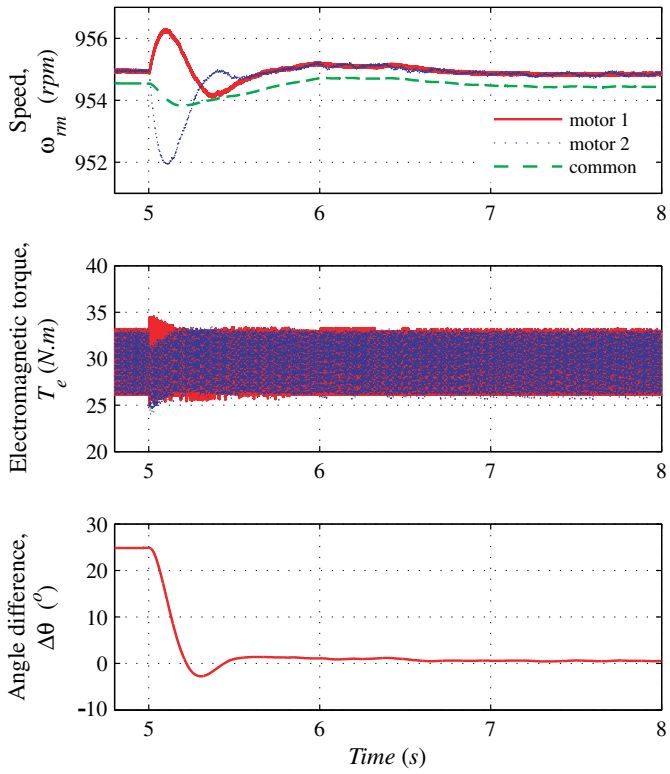

Fig. 9. Speed, electromagnetic torque, and angle transient of proposed SLC.

D. *Emulated Driving Condition*

To demonstrate the motor drive system operation under uneven road conditions, in this subsection the system is subjected to a simple torque load profile shown in Fig. 13

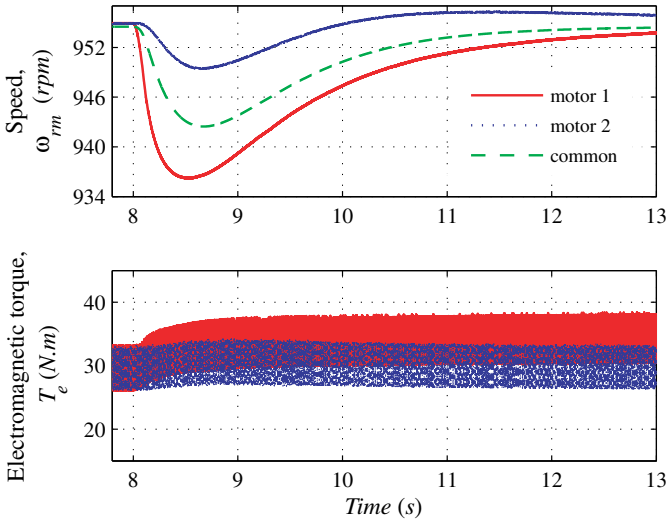

Fig. 10. Speed and electromagnetic torque transient response due to load change with conventional EDS.

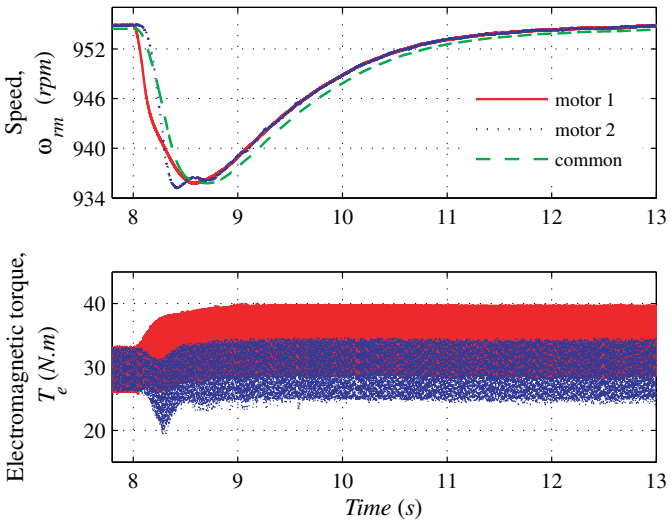

Fig. 11. Speed and electromagnetic torque transient response due to load change with proposed SLC.

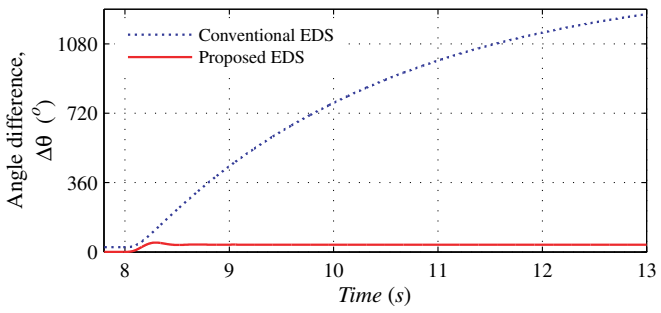

Fig. 12. Difference in motor angles using conventional and proposed approaches.

(top). This torque profile is considered to emulate a bumpy road condition that imposes different stresses on the vehicle's wheels. As can be seen in Fig. 13 (second subplot), there is a significant difference in the instantaneous speed of the shafts/wheels when the conventional EDS is used. This is also observed in Fig. 13 (fourth subplot), which shows the difference between the shafts' angles. However, the proposed SLC achieves very good locking of the shafts and the speeds as depicted in Fig. 13.

V. CONCLUSION

This paper presented a simple and effective locking technique to be incorporated into the differential system of the electric vehicle with independent brushless DC (BLDC) machine-based wheel drives. The new approach is based on averaging the Hall sensor signals and applying the same averaged switching intervals to both propulsion motors. The proposed SLC improves the performance of the vehicle under certain road conditions compared to the conventional EDS.

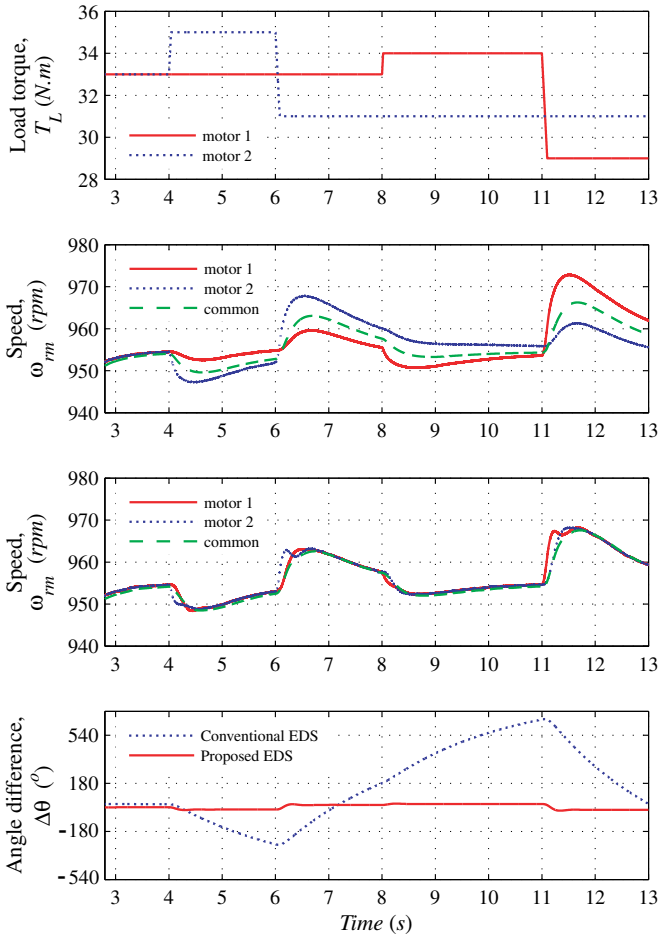

Fig. 13. Load profile response of the conventional EDS and proposed SLC.

APPENDIX A

BLDC PROPULSION MOTOR PARAMETERS:

eCycle Inc., Model MGA-1-13, 4.5 kW, 12 poles, $r_s = 0.027\Omega$, $L_s = 0.025mH$, $\lambda_m^{'} = 10.9mV.s$, rotor inertia $J_{rot} = 0.005kg.m^2$, back EMF harmonics coefficients $K_3 = -0.206$, $K_5 = 0.047$, $K_7 = -0.0067$.

MECHANICAL PARAMETERS:

Mass of the vehicle, $M_v = 190kg$, mass of the wheel, $M_w = 10kg$, load inertia, $J_{load} = 0.02kg.m^2$, damping coefficient, $B_m = 0.05N.s$, radius of the wheel, $r = 0.05m$, gravitational constant, $g = 9.81m/s^2$, and controller coefficients $K_p = 0.012$, $K_i = 0.0161$.

ACKNOWLEDGMENT

This work was supported in part by the Institute for Computing, Information and Cognitive Systems (ICICS) at UBC. We thank Kamran Tabarraee and Jaishankar Iyer for their help in carrying out experiments.

REFERENCES

[1] M.Ehsani, Y.Gao, S.E.Gay, and A.Emadi. *Modern Electric Hybrid Electric, and Fuel Cell Vehicles: Fundamentals, Theory, and Design*. CRC Press, Boca Raton, FL, 2005.

[2] P. C. Krause, O. Wasynczuk, S. D. Sudhoff. *Analysis of Electric Machinery and Drive Systems*. IEEE Press, Piscataway, NJ, 2002.

[3] S. D. Sudhoff, P. C. Krause, "Average-value Model of the Brushless DC 120º Inverter System," *IEEE Transactions on Energy Conversion, Vol. 5, No. 3, pp. 553-557, 1990.*

[4] S. D. Sudhoff, P. C. Krause, "Operation Modes of the Brushless DC Motor with a 120º Inverter," *IEEE Transactions on Energy Conversion, Vol. 5, No. 3, pp. 558-564, 1990.*

[5] P. L. Chapman, S. D. Sudhoff, C. A. Whitcomb, "Multiple Reference Frame Analysis of Non-sinusoidal Brushless DC Drives," *IEEE Transactions on Energy Conversion, Vol. 14, No. 3, pp. 440-446, 1999.*

[6] *Simulink: Dynamic System Simulation for MATLAB, Using Simulink Version 7.3*, The MathWorks Inc., 2009a.

[7] *Automated State Model Generator (ASMG), Reference Manual Version 2*, P.C. Krause & Associates, Inc. 2003.

[8] P. Pillay, R. Krishnan, "Modeling, simulation, and analysis of permanent-magnet motor drives. Part II. The brushless DC motor drive," *IEEE Transactions on Industry Applications,* Vol. 25, Iss. 2, March-April 1989, pp. 274-279.

[9] W. Brown, "Brushless DC Motor Control Made Easy", Microchip Technology Inc., 2002. [Online]. Available: www.microchip.com

[10] N. Samoylenko, H. Qiang, J. Jatskevich, "Dynamic Performance of Brushless DC Motors with Unbalanced Hall Sensors," *Energy Conversion, IEEE Transactions on*, vol.23, no.3, pp.752-763, Sept. 2008.

[11] W-S.Kim, Y-S.Kim, J-K.Kang, and S-K.Sul, "Electro-mechanical re-adhesion control simulator for inverter-driven railway electric vechicle", *Conference Record of the 1999 IEEE Industry Applications Conference*, 2:1026-1032, 1999.

[12] Y. Takaoka, A. Kawamura, "Disturbance Observer Based Adhesion Control for Sinkansen", *AMC2000-NAGOYA*, *2000*, pp.169-174.

[13] B. Tabbache, A. Kheloui, N. Hanini, "An electric differential system for a two-wheel mobile plat-form using direct torque control with adaptive flux and speed observers," *Power Electronics, Electrical Drives, Automation and Motion, 2008. SPEEDAM 2008. International Symposium on* , vol., no., pp.550-556, 11-13 June 2008